TISSUE ENGINEERING: Part A
Volume 21, Numbers 11 and 12, 2015

DOI: 10.1089/ten.tea.2014.0497

Effect of Local Sustainable Release of BMP2-VEGF from Nano-Cellulose Loaded in Sponge Biphasic Calcium Phosphate on Bone Regeneration

Mousumi Sukul, MS,[1] Thuy Ba Linh Nguyen, PhD,[1,2] Young-Ki Min, MD,[2,3] Sun-Young Lee, PhD,[4] and Byong-Taek Lee, PhD[1,2]

Bone regeneration is a coordinated process mainly regulated by multiple growth factors. Vascular endothelial growth factor (VEGF) stimulates angiogenesis and bone morphogenetic proteins (BMPs) induce osteogenesis during bone healing process. The aim of this study was to investigate how these growth factors released locally and sustainably from nano-cellulose (NC) simultaneously effect bone formation. A biphasic calcium phosphate (BCP)-NC-BMP2-VEGF (BNBV) scaffold was fabricated for this purpose. The sponge BCP scaffold was prepared by replica method and then loaded with 0.5% NC containing BMP2-VEGF. Growth factors were released from NC in a sustainable manner from 1 to 30 days. BNBV scaffolds showed higher cell attachment and proliferation behavior than the other scaffolds loaded with single growth factors. Bare BCP scaffolds and BNBV scaffolds seeded with rat bone marrow mesenchymal stem cells were implanted ectopically and orthotopically in nude mice for 4 weeks. No typical bone formation was exhibited in BNBV scaffolds in ectopic sites. BMP2 and VEGF showed positive effects on new bone formation in BNBV scaffolds, with and without seeded stem cells, in the orthotopic defects. This study demonstrated that the BNBV scaffold could be beneficial for improved bone regeneration. Stem cell incorporation into this scaffold could further enhance the bone healing process.

Introduction

Bone is a highly vascularized tissue within the body with a unique capacity to heal and remodel constantly.[1] Depending on this regenerative capacity, various types of grafts have been traditionally used to restore large bone defects.[2] Use of porous ceramic scaffolds has been a longstanding area of interest in the field of research. Biphasic calcium phosphate (BCP) porous sponge scaffold has been widely used for this purpose. It consists of a mixture of hydroxyapatite (HAp) [$Ca_{10}(PO_4)_6(OH)_2$], and β-tricalcium phosphate (β-TCP) [β-$Ca_3(PO_4)_2$], which mimics the structure of natural cancellous bone and has gained much attention for its excellent biocompatibility and biodegradability.[3] However, as a drug delivery system, these scaffolds alone are not efficient enough to keep drugs at the site for a long duration, resulting in a faster release.[4] Drugs should be efficiently entrapped in the scaffolds to be released for a prolonged period. Use of a suitable polymer hydrogel as a drug carrier, together with the porous osteoconductive frame, can provide a better system to accelerate bone healing mechanism.

Hydrogels are emerging group of materials for tissue regeneration.[5–11] Hydrogels from both synthetic and natural sources and of various kinds that is, polysaccharides, polypeptides, and composites, have been used in this field. Water-soluble polysaccharides require different cross-linking steps to form a stable structure.[12] Instead of being soluble, bacteria and plant[6]-derived nano-cellulose (NC) form colloidal dispersions in water. They have mechanically strong nanostructures[13] with a slow degradation rate.[14] NC limits drug diffusion by forming a tight fiber network, thereby sustaining drug release.[15] Bacterial cellulose scaffolds have already proven their potentiality for bone and cartilage tissue engineering.[6,16] However, very few applications have been found for plant-derived NC, to date. Nano-level fibrous structure of plant-derived NC may help to entrap the growth factors and its low degradation behavior may help in their sustained release.

Growth factors are soluble signaling molecules that stimulate cell growth, migration, differentiation, and angiogenesis.[17–22] Bone regeneration process is accomplished by the active participation of different growth factors.

[1]Department of Regenerative Medicine, College of Medicine, Soonchunhyang University, Cheonan, Republic of Korea.
[2]Institute of Tissue Regeneration, College of Medicine, Soonchunhyang University, Cheonan, Republic of Korea.
[3]Department of Physiology, College of Medicine, Soonchunhyang University, Cheonan, Republic of Korea.
[4]Division of Environmental Material Engineering, Department of Forest Products, Korea Forest Research Institute, Seoul, Republic of Korea.

Among them, bone morphogenetic proteins (BMPs) play the most effective role by initiating the different stages of bone development, including the recruitment of mesenchymal stem cells (MSCs) and their transformation to osteoblasts.[23] Together with osteogenesis, angiogenesis is also a crucial process for bone regeneration. Newly formed blood vessels by angiogenesis provide nutrient supply and transportation of essential macromolecules to the defect site.[24] Endothelial cells in close contact with stem cells can influence their proliferation and differentiation.[25] Vascular endothelial growth factor (VEGF), along with its osteoinductive properties,[19] is a potent inducer of angiogenesis.[26] According to a previous report, delivery of exogenous VEGF enhanced BMP2-induced bone formation.[27] Several studies reported that dual delivery of BMP2 and VEGF showed better and more efficient bone regeneration than single growth factor delivery.[27–29] However, to induce bone formation, it is necessary to deliver growth factors effectively so that they can retain their activity at the defect site.[30]

The initial stage of osteoinduction process includes the recruitment of MSCs. Application of MSCs showed enhanced bone formation in hydroxyapatite scaffolds in critical size defects in the sheep,[31] in the ectopic rat model seeded in a β-TCP fibrin glue mixture[32] and in BCP scaffolds in the ectopic mouse model.[33] Release of BMP2-VEGF in close proximity to MSCs from a three-dimensional (3D) scaffold provides a suitable strategy for bone augmentation.[34]

In this study, we developed a new 3D scaffold system that offers a sustainable growth factor release kinetic along with its osteoconductive porous frame. The porous sponge BCP scaffold was loaded with BMP2-VEGF incorporated NC. Growth factors were physically entrapped in the nano-level fibrous structure of the slow degradable NC. Material properties of the scaffolds were investigated, and their *in vitro* properties were evaluated using rat bone marrow mesenchymal stem cells (RBMSCs) and *in vivo* experiments were carried out with nude mouse ectopic and orthotopic implantation. We investigated the VEGF and BMP-2 release profiles from the scaffolds, their effects on *in vitro* proliferation and differentiation of RBMSCs, and ectopic and orthotopic bone formation efficiency in nude mice seeded with RBMSCs.

Materials and Methods

Fabrication of scaffolds

Preparation of 0.5% NC solution. 0.5% aqueous solution of NC was obtained from the Korea Forest Research Institute. It was prepared by a high pressure homogenization process.[35]

Fabrication of BCP-NC-BMP2-VEGF scaffolds. BCP scaffold was fabricated by sponge replica method.[36] As a starting material, nano-sized BCP powder, which was synthesized by microwave-assisted process,[37] polyvinyl butyral (Butvar® B-98; Acros) as a binder, and PU foam (45 ppi, 3 M) were used. At first 3% of polyvinyl butyral was mixed with ethanol (Merck) and stirred for 2 h to prepare BCP slurry, and subsequently 25% of synthesized nano powder was added, and stirred for additional 6 h. Prepared PU foam was immersed in the prepared slurry and dried. The process was repeated four times. The coated PU foam was then sintered at 1350°C for 10 min. Fabricated BCP scaffolds were washed with distilled water under ultrasonication to remove impurities, especially, from the internal porous structure. Before incorporation, both BCP scaffolds and NC were autoclaved at 121°C for 20 min to maintain the microbial purity.[10] About 0.5% aqueous solution of NC was taken in a pipette and dropped slowly on the scaffolds under vacuum and kept on a shaker for 8 h at 4°C; during this time they were turned upside down several times to ensure proper loading. rhBMP2 (Recombinant BMP2; R&D systems) and rhVEGF (recombinant VEGF; R&D systems) were added to the NC solution at the concentrations of 10 μg/mL before loading. The entire loading process was performed under a laminar flow hood to avoid contamination. Loaded scaffolds were subsequently frozen at −80°C for 4 h. After freezing, the scaffolds were freeze-dried for 24 h and kept in a sealed container at 4°C for further studies.

Characterization of scaffolds

Morphological analysis. The morphologies of the scaffolds were evaluated using scanning electron microscopy (SEM, JSM701F; JEOL). Before scanning, the scaffolds were placed on the SEM sample holder and sputter coated with platinum (Cressington Scientific Instruments). All micrographs were taken at an acceleration voltage of 10 kV.

Porosimetry. Mercury intrusion porosimetry (poreMaste™; Quantachrome Intruments) and micro-computed tomography (Micro-CT, Skyscan 1076; Skyscan) were used to analyze porosity. Low pressure intrusion porositymetry was used to obtain interconnected pore diameter and porosity. For micro-CT analysis, each sample was fixed on the object stage and imaging was performed on the sample for 360° of rotation with an exposure time of 20 min. Micro-CT images were reconstructed over the region of interest using CTAn (Skyscan) and CTVol (Skyscan) to make 3D images and then, porosity was calculated.

Mechanical properties. Compressive strength was determined using a universal testing machine (Unitech TM; R&B) with a 1 kN load cell at room temperature. The crosshead speed was 0.5 mm/s. All samples were prepared in a rectangular shape with dimensions of $5 \times 5 \times 7$ mm.

BMP2-VEGF release profiles. *In vitro* single or combined growth factor release from the scaffolds was calculated. Scaffolds loaded with BMP2 and/or VEGF were placed in 24-well cell culture plates and 200 μL of media were added to each well and incubated in a CO_2 incubator (ASTEC). The total doses of BMP2 and/or VEGF initially loaded onto scaffolds were the same (10 μg/mL). The extracts were collected at 1, 3, 5, 7, 10, 14, 17, 21, and 30 days. Then, the release of BMP2 and VEGF was measured using the Human BMP2 release kit (Quantikin ELISA; R&D systems) and Human VEGF release kit (Quantikin ELISA; R&D systems), respectively. The optical density (OD) values were measured using an ELISA reader (EL, 312, Biokinetics reader; Bio-Tek instruments) at wavelengths of 540 and 450 nm. The amount of growth factors released were then calculated and expressed as the cumulative percentages of loading.

In vitro *studies*

Isolation and cultivation of RBMSCs. Cancellous bone was removed from femurs of 3-week-old rats (Samtako; Bio Korea) and washed thrice with phosphate-buffered saline (PBS). The bone marrows were flushed out and filtered through a cell strainer filter (100 μm nylon; Falcon), pooled, and centrifuged at 1500 rpm for 5 min to remove the supernatants. The cell pellet was resuspended in minimum essential medium-alpha (MEM-α; Gibco) supplemented with 10% fetal bovine serum (Gibco) and 1% penicillin/streptomycin. Cells were suspended in 5% acetic acid to remove the red blood cells, and mononuclear cells were counted by trypan blue exclusion. About 1.0×10^7 cells were seeded in a culture dish (ϕ 150) and cultured for 10–14 days as a monolayer in a humidified incubator at 37°C in an atmosphere of 95% air and 5% CO_2. Third passage cells were used in subsequent cultures.[38,39]

Cell adhesion. Before cell seeding, the scaffolds were sterilized under UV light, washed with PBS, and finally soaked in MEM-α. Sterilized scaffolds seeded with 1×10^5 cells/mL were incubated for 2 and 4 h in 24-well cell culture plates. The cells on the scaffolds were fixed with 4% paraformaldehyde (Sigma-Aldrich). The cells were permiabilized in 0.5% Triton X-100 (Sigma-Aldrich) and blocked with 2.5% bovine serum albumin for nonspecific binding. Focal adhesions were visualized by staining with mouse monoclonal anti-vinculin (1:50 dilutions; Millipore) at 4°C overnight. Next, the cells were stained with F-actin labeled with Alexa 594-coupled phalloidin (1:50 dilutions; Molecular Probe) for 30 min. Nuclei were counterstained with Hoechst 33342 (Sigma). Micrographs were visualized under a confocal fluorescent microscope (FV10i-W).

Cell viability. After the RBMSCs reached a confluence of 70–80% in the subculture plate, the cells were trypsinized (trypsin-EDTA; Gibco), detached, and counted. Approximately, 10^5 cells/mL of media were seeded on the scaffolds in 24-well plates. The plates were then incubated in a CO_2 incubator for 1, 3, and 7 days. One hundred microliters of MTT (3-[4,5-dimethyl-2-thiazolyl]-2,5-diphenyltetrazolium bromide; Sigma-Aldrich) solution was added to each well on each sampling day. MTT produced purple-colored formazan crystals reacting with cellular dehydrogenase at the bottom of each well. After 4 h of incubation, 1 mL dimethyl sulfoxide (Samchun Pure Chemical Co.) was added to each well to solubilize the formazan. The OD values of the solution were measured using an ELISA reader (EL, 312, Biokinetics reader; Bio-Tek instruments) at a wavelength of 595 nm. The OD corresponds to the number of viable cells.

Cell proliferation. Scaffolds seeded with RBMSCs at a density of 1×10^5 cells/mL were incubated for 1 and 7 days in 24-well cell culture plates. At each sampling day the scaffolds with cultured cells were washed with PBS (Amresco) solution and cells were fixed, permeabilized, and blocked for nonspecific binding. Cells were immunostained with fluorescein isothiocyanate (FITC)-conjugated phalloidin (25 μg/mL; Sigma) overnight at 4°C. Nuclei were counterstained with 1 μg/mL of Hoechst 33342. The scaffolds were visualized under a confocal fluorescent microscope (FV10i-W; Olympus) and images were analyzed using accompanying FV10i-ASW 3.0 Viewer software.

Cell differentiation. Scaffolds were seeded at 1×10^5 cells/mL and incubated for 7 and 14 days. Before staining cells were fixed, permeabilized, and blocked for nonspecific binding. The following antibodies were used for immunostaining: Alkaline Phosphatase-H-300 (1:50 dilutions; Santa Cruz) overnight and Alexa Fluor-488-conjugated goat anti-rabbit IgG (H + L; Invitrogen) for 1 h for visualizing alkaline phosphatase (ALP) activity; OPN-AKm2A1(1:50 dilutions; Santa Cruz) overnight and Alexa Fluor-488-conjugated goat anti-mouse IgG (H + L; Invitrogen) for 1 h for visualizing osteopontin activity; in combination with Alexa 594-conjugated goat anti-rabbit IgG antibodies (Invitrogen). Nuclei were counterstained with Hoechst 33342. The scaffolds were visualized under a confocal fluorescent microscope (FV10i-W; Olympus).

Reverse transcriptase–polymerase chain reaction. About 1×10^5 cells/mL were seeded on each scaffold and incubated for 7 and 14 days in 12-well culture plates using osteogenic medium. RBMSCs were collected from the scaffold's surface using trypsin-EDTA. Total RNA was extracted from cultured cells using TRIzol reagent (Invitrogen) according to the manufacturer's recommended protocol. The RNA was quantified by UV-spectrophotometry. Extracted RNA (1 μg) was used for the first strand cDNA synthesis (iScript cDNA synthesis kit; Bio-Rad). Then, 1 μL of the synthesized cDNA was used as a template for amplification of RNA samples. The samples were subjected to reverse transcriptase–polymerase chain reaction (RT-PCR) using iQ SYBR Green Supermix (Bio-Rad) with three primer pairs (ALP, osteopontin [OPN], and osteocalcin [OCN]). RT-PCR was carried out under the following parameters: 95°C for 5 min, 95°C for 30 s, 58°C for 30 s, 72°C for 30 s (40 cycles), 72°C for 5 min, 65°C for 5 s, and a final cycle at 95°C. Glyceraldehyde-3-phosphate dehydrogenase (GAPDH) was used as the internal control.[40] The primers used in this study were listed in Table 1.

In vivo *study*

Implantation of the scaffolds in nude mice. Nude mouse strain was selected to avoid any potential immune response to the scaffolds or RBMSCs. A total of 15 Balb-C (25 g; Dayoon) mice were used in this study. All *in vivo* procedures

Table 1. Primer Sequences Used for the Detection of Genes

Genes	*Primers*
ALP	F: 5′-GACAAGAAGCCCTTCACAGC-3′
	R: 5′-ACTGGGCCTGGTAGTTGTTG-3′
OPN	F: 5′-GATCGATAGTGCCGAGAAGC-3′
	R: 5′-TGAAACTCGTGGCTCTGATG-3′
OCN	F: 5′-AGCTCAACCCCAATTGTGAC-3′
	R: 5′-AGGGTCGAGTCCTGGAGAGT-3′
GAPDH	F: 5′-AAGTTCAACGGCACAGTCAA-3′
	R: 5′-TACTCAGCACCAGCATCACC-3′

ALP, alkaline phosphatase; *GAPDH*, glyceraldehyde-3-phosphate dehydrogenase; *OCN*, osteocalcin; *OPN*, osteopontin.

were performed in accordance with the protocol approved by the Animal Ethical Committee of Soonchunhyang University for the care and use of laboratory animals. The mice were anesthetized with diethyl ether (Daejung). Antisepsis was provided with povidone iodine. For assessment of ectopic bone formation, two small paravertebral incisions of 10 mm long were made on the dorsum of each mouse where single implants were placed. Before implantation, RBMSCs were differentiated on the scaffolds using osteogenic media. The animals were assigned to one experimental and one control group with three animals in each group. For orthotopic implantation, animals were divided into three groups (two experimental and one control group) with three animals in each group. A midline incision was made on the skull skin. After elevating cranial skin flaps, a 3 mm hole was made with a trephine drill penetrating through the calvarial bone. Constant saline irrigation was provided during drilling, and extreme care was taken not to injure the dura mater. Defects were grafted with different groups of scaffolds including control. The incisions were closed with 5–0 mononylon simple sutures. The mice were sacrificed at 4 weeks of implantation and the ectopic and orthotopic implants were collected.

Micro-CT. The extracted samples were fixed in a 10% formalin solution for micro-CT analysis and histopathology study 4 weeks postimplantation. Micro-CT was used to observe the new bone formation in the scaffolds. After reconstruction of micro-CT images, DataViewer (Skyscan), CTAn (Skyscan), and CTVol (Skyscan) were used to make two-dimensional (2D) and 3D images. Percent bone volume (bone volume [BV]/tissue volume [TV]%) were calculated to measure the new bone volume.

Histology. After the micro-CT analysis, formalin-fixed samples were decalcified using 5% nitric acid. The decalcified samples were embedded in paraffin wax and cut

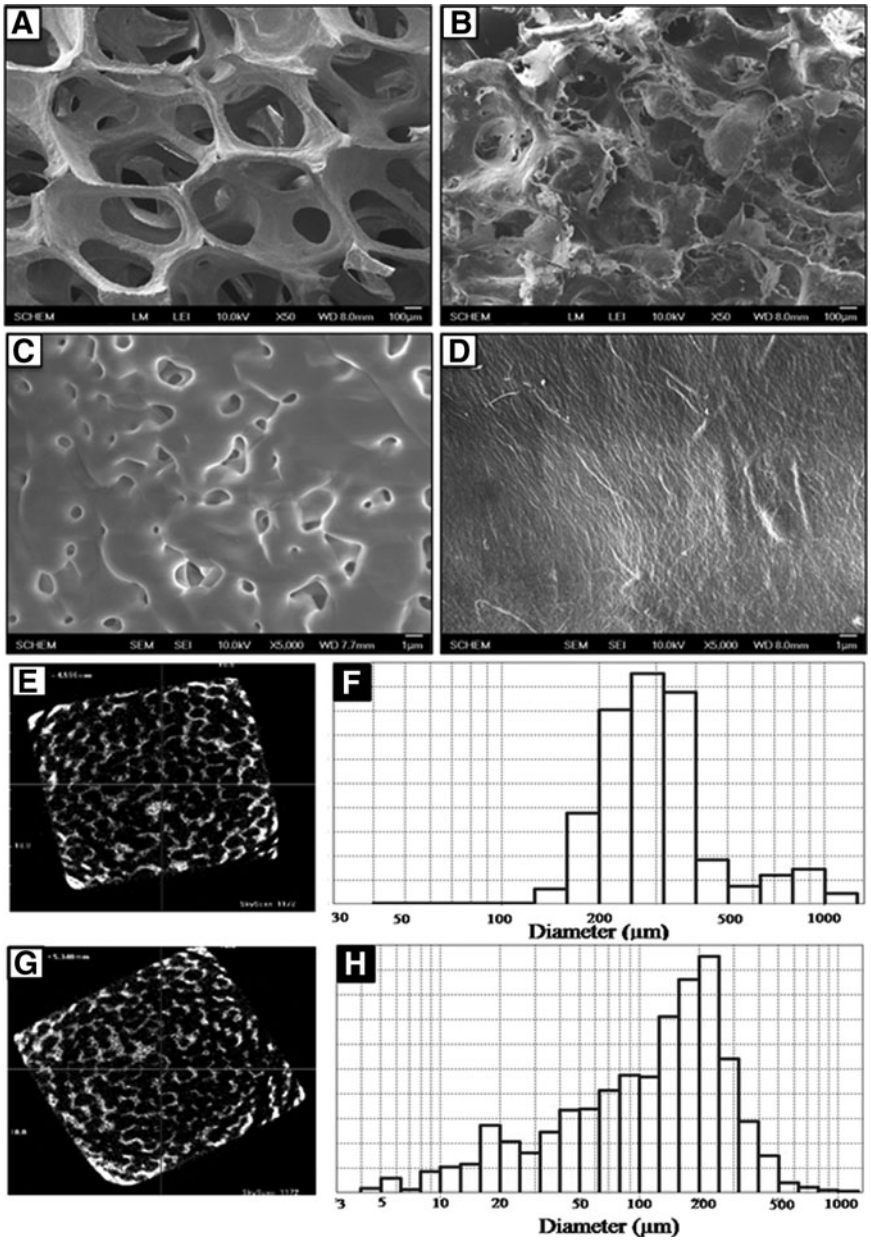

FIG. 1. The morphologies of BCP **(A, C)** and BN **(B, D)** scaffolds were evaluated by scanning electron microscope. Porosity was analyzed by micro-CT and mercury porosimetry of BCP **(E, F)** and BN **(G, H)** scaffolds, respectively. BCP, biphasic calcium phosphate; BN, BCP-NC; NC, nanocellulose.

using a microtome (HM 325; Thermo Scientific). The 4 ± 2 μm thick sections were mounted on microscope slides. The sections were stained with hematoxylin and eosin and Masson's trichrome. Tissue sections were viewed with an Olympus BX53 light microscope and photographed with an Olympus DP72 camera. Images were analyzed using the accompanying Cellsens software.

Statistical analysis

The results were statistically analyzed using one-way and two-way analysis of variance with *post hoc* correction (Bonferroni method). Analyses were carried out using GraphPad Prism 5 with a confidence level of $p < 0.05$ unless stated otherwise to determine the statistical significance of data obtained from the experiments.

Results

Characterization of scaffolds

Morphological characterization. Figure 1 showed the micrographs of bare BCP and BCP-NC (BN) scaffolds. The low magnification SEM (Fig. 1A, B) and micro-CT images (Fig. 1E, G) showed the interconnected porous structures of the scaffolds. The bare BCP scaffold showed porous structures with an average of 350 μm with a maximum of ~1000 μm pores (Fig. 1A, F). After NC loading the pore size of the NC-BCP scaffolds decreased to an average of 250 μm (Fig. 1B, H). The high magnification images (Fig. 1C, D) showed the surface topography of the scaffolds. Bare BCP scaffold (Fig. 1C) showed fusion of the BCP particles and free spaces between the nonfused particles created microporosity. The loaded NC considerably reduced microporous structures of the scaffold (Fig. 1D) providing a smooth surface. This image also showed the fibrous structure of NC.

The average pore size, porosity distribution, and compressive strength of the scaffolds were listed in Table 2. The pore size of the bare BCP scaffold ranged from 200 to 350 μm with a porosity of 92%, whereas NC-BCP scaffolds had pores ranging from 150 to 250 μm with 86.8% porosity. The bare BCP scaffolds showed low compressive strength of about 1.02 MPa. After loading of cellulose the compressive strength increased up to 2.40 MPa.

Release of BMP2-VEGF. The *in vitro* growth factor-releasing properties of the scaffolds were measured by quantitative ELISA. Extract samples were collected up to 30 days (Fig. 2). Initial releases of BMP2 were 3.19% and 3.67% and total amounts of 31.92% and 31.90% of BMP2 were released from BCP-NC-BMP2 (BNB) and BCP-NC-BMP2-VEGF (BNBV) scaffolds, respectively, over the time period of 30 days. VEGF release was higher at the initial stage at 7.91% and a total amount of 47.75% VEGF was released from BCP-NC-VEGF (BNV) scaffolds while the initial release was reduced to 4.68% when it was released from BNBV scaffolds. Totally, 33.38% of VEGF was released from these scaffolds after the same period of time. A slow and steady release was found when the growth factors were released from dual growth factor containing scaffolds.

Table 2. Characterization of Bare Biphasic Calcium Phosphate and Nano-Cellulose–Biphasic Calcium Phosphate Scaffolds

Name of the samples	*Pore size (μm)*	*Porosity (%)*	*Compressive strength (MPa)*
Bare BCP	200–350	92.0 ± 0.08	1.02 ± 0.10
NC-BCP	150–250	86.8 ± 0.05	2.40 ± 0.08

Data represent mean ± standard deviation.
BCP, biphasic calcium phosphate; NC, nano-cellulose.

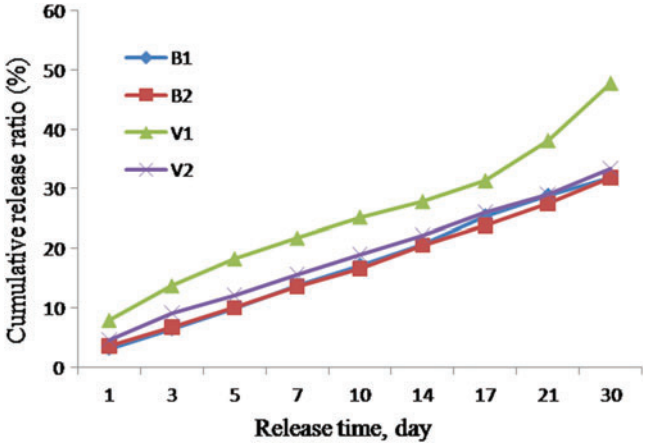

FIG. 2. Graph showing BMP-2 and VEGF release profiles. B1, BMP2 released from BNB scaffolds; B2, BMP2 released from BNBV scaffolds; V1, VEGF released from BNV scaffolds; V2, VEGF released from BNBV scaffolds. BMP, bone morphogenetic protein; BNB, BCP-NC-BMP2; BNBV, BCP-NC-BMP2-VEGF; BNV, BCP-NC-VEGF; VEGF, vascular endothelial growth factor. Color images available online at www.liebertpub.com/tea

In vitro *cytocompatibility*

RBMSCs were used to assess the biocompatibility of the fabricated scaffolds. The adhesion behavior was investigated after 2 and 4 h of cell seeding. Figure 3A showed that cells were rounded and did not attach to the surface of the scaffolds in every case after 2 h of cell seeding, however, after 4 h cells exhibited rounded nuclei and spread morphology with the appearance of actin filaments. The staining of vinculin (green) showed small punctate focal adhesions across the cell body on the scaffolds. Cells were more spread on BNB, BNV, and BNBV scaffolds. It was evident from the Figure 3A that BMP2 and VEGF promoted cell adhesion.

MTT assay showed that RBMSCs continuously proliferated on the scaffolds without exhibiting any negative effect on their growth rate. Growth pattern depicted that cells grew better in all scaffolds containing growth factor and dual growth factors had a positive effect on cell proliferation rate. After 7 days of culture, cell proliferation was highest on BNBV scaffolds (Fig. 3B).

Figure 3C showed confocal micrographs of RBMSCs on the scaffolds after 1 and 7 days of culture. After 1 day of incubation, the cells were well attached on the surface of all scaffolds. Comparison with cell proliferation data revealed that a higher number of cells were attached to BNB, BNV,

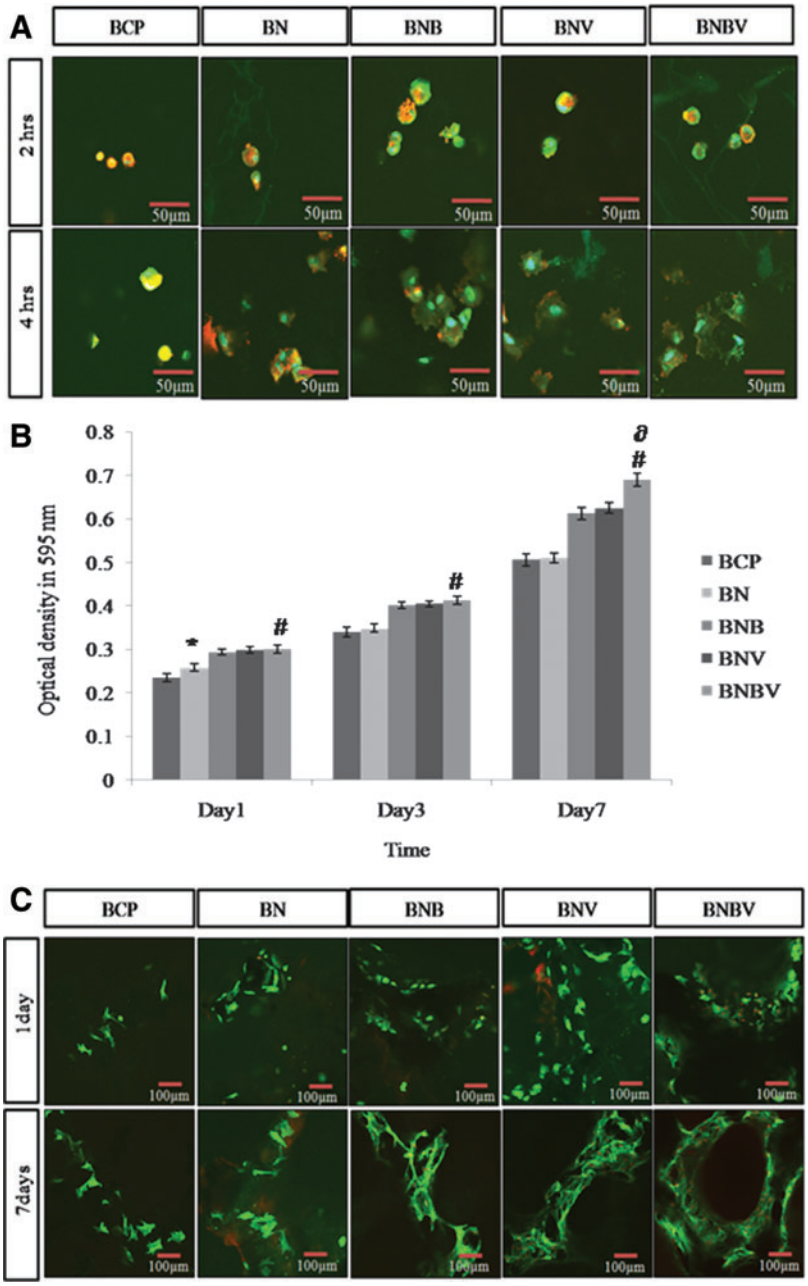

FIG. 3. **(A)** Cell adhesion behavior after 2 and 4 h of culture of RBMSCs on different scaffolds was observed by confocal microscopy with triple stain of cell nucleus (*blue*), actin fibers (*red*), and the focal adhesion protein vinculin (*green*). **(B)** Viability and proliferation of RBMSCs on different scaffolds were determined by **(B)** MTT assay and **(C)** F-actin staining. $^{*}p < 0.05$ versus BCP scaffolds, $^{\#}p < 0.001$ versus BCP scaffolds, $^{\partial}p < 0.001$ versus BNB and BNV scaffolds. RBMSCs, rat bone marrow mesenchymal stem cells. Color images available online at www.liebertpub.com/tea

and BNBV scaffolds. At 7 days, there was a dense cellular mass of RBMSCs with multiple layers on the scaffolds. Highest biocompatibility was observed on BNBV scaffolds. Generally, cells on all growth factor-containing scaffolds showed enhanced cell proliferation than bare BCP or BN scaffolds, indicating that drug releasing behavior of NC was beneficial for cell growth.

The activities of ALP and OPN, key markers of osteogenic differentiation were analyzed (Fig. 4). The analysis was performed after 7 and 14 days of culture in osteogenic medium. Immunostaining was performed for protein localization in RBMSCs, which was visualized by confocal microscopy. Specific antibodies were applied to tag ALP and OPN proteins expressed in the cells. At 7 days, cells showed a higher level of ALP activity (green) on BNBV scaffolds than BNB and BNV scaffolds (Fig. 4A). At 14 days, cells on BNB scaffolds showed higher ALP activity than on BNV scaffolds and it was more intense on BNBV scaffolds (Fig. 4B). Assessment of OPN activity also exhibited similar results (Fig. 4C, D). At 14 days, the green color representing OPN expression in cells on BNBV scaffolds was distinctly more intense than on any other scaffolds (Fig. 4D).

To study the osteoblastic gene expression RT-PCR was performed (Fig. 5). The expression of *ALP*, *OPN*, and *OCN* mRNAs in RBMSCs were quantified after 7 and 14 days of culture. At 7 days, both early stage markers (*ALP* and *OPN*) and late stage marker (*OCN*) were expressed on all of the scaffolds. Gene expressions were better on the scaffolds loaded with growth factors than BCP and BN scaffolds. At 7 days, there was no significant difference in *ALP* and *OPN*

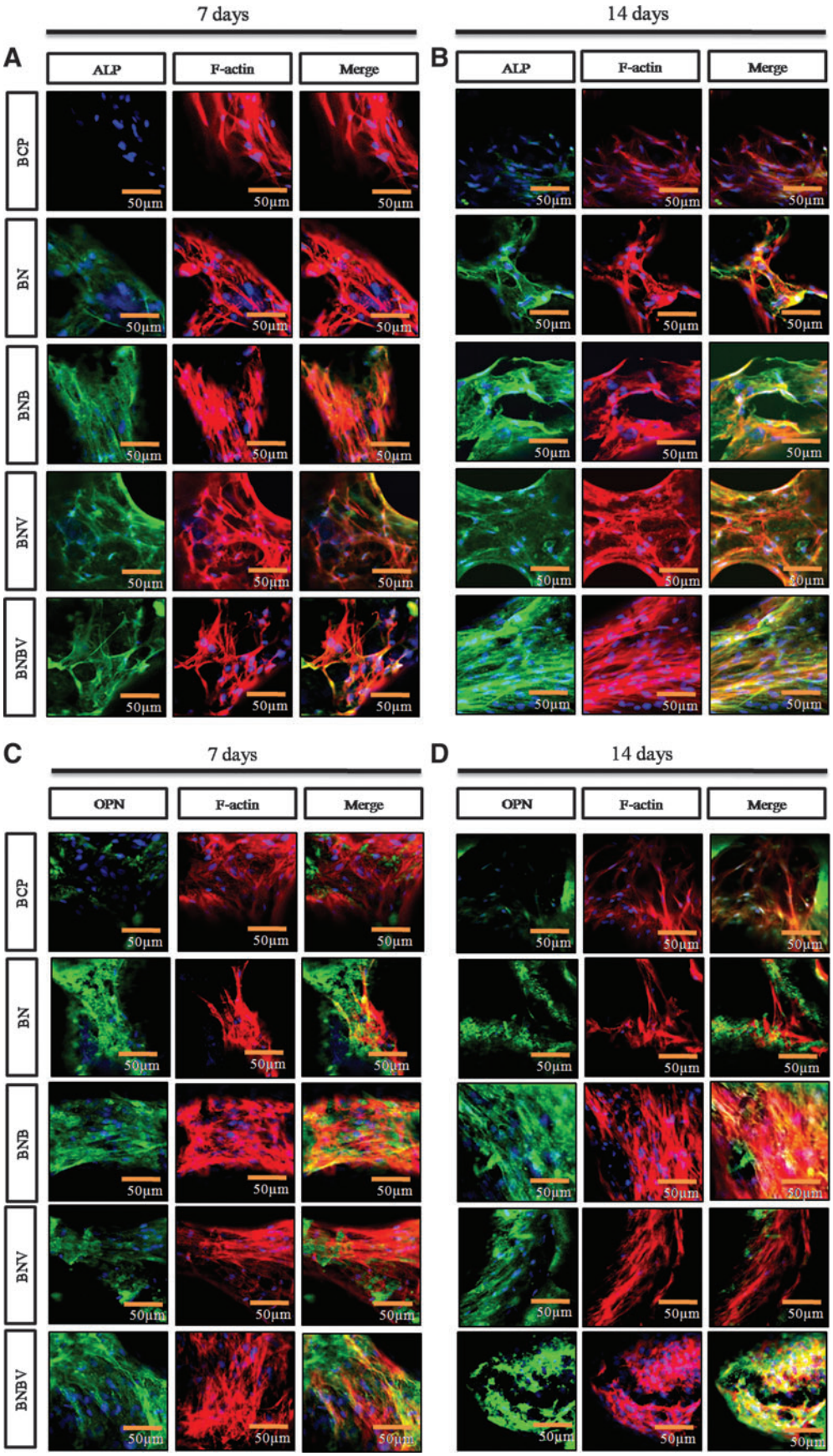

FIG. 4. Confocal micrographs depicting cell differentiation behavior of RBMSCs on the scaffolds to explore the effect of released growth factors. Immunostained images are showing the ALP **(A, B)** and OPN **(C, D)** protein localization (*green*) in RBMSCs at 7 days **(A, C)** and 14 days **(B, D)**. ALP, alkaline phosphatase; OPN, osteopontin. Color images available online at www.liebertpub.com/tea

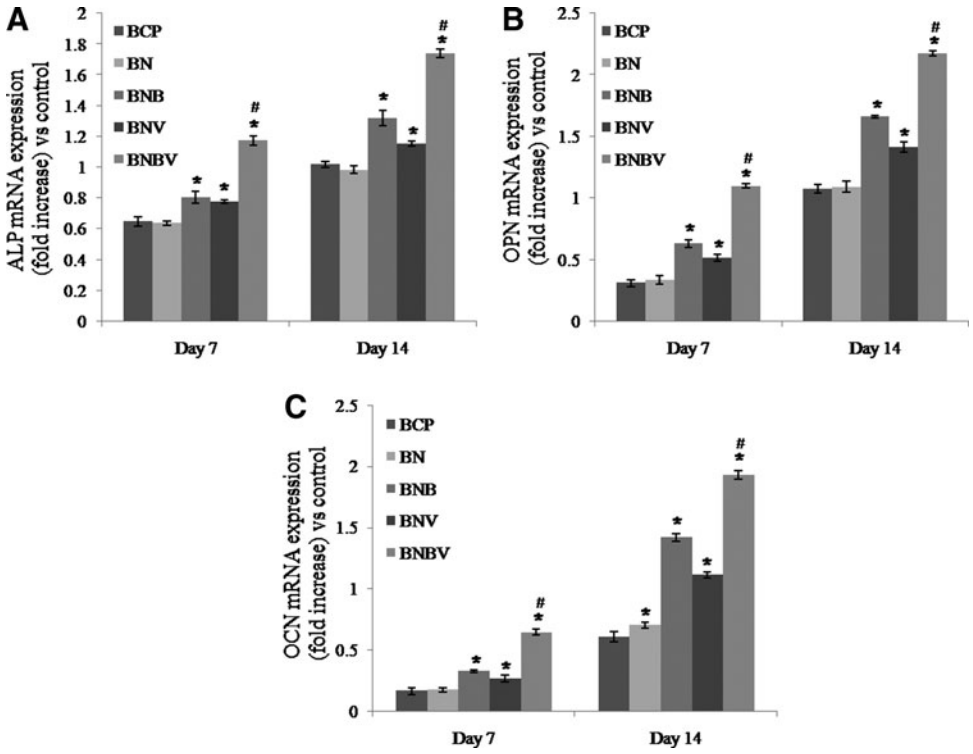

FIG. 5. Representative histograms of *ALP* **(A)**, *OPN* **(B)**, and *OCN* **(C)** mRNA expressions in RBMSCs grown on the surface of the scaffolds at 7 and 14 days analyzed by reverse transcriptase–polymerase chain reaction. Expressions were normalized to GADPH (control gene). $^{*}p<0.001$ versus BCP scaffolds, $^{\#}p<0.001$ versus BNB and BNV scaffolds. *OCN*, osteocalcin.

gene expression in BNB and BNV scaffolds but at 14 days, BNB scaffolds showed better gene expressions than BNV scaffolds. *ALP* and *OPN* gene expressions were higher on BNBV scaffolds than BNB and BNV scaffolds at 7 days and fold difference increased at 14 days (Fig. 5A, B). At 7 days, *OCN* gene expression was lower than *ALP* and *OPN* genes on all of the scaffolds but the expression was upregulated at 14 days. The highest *OCN* gene expression was observed in BNBV scaffolds at both time periods (Fig. 5C). These results confirmed positive effect of combined release of BMP2 and VEGF from BNBV scaffolds on osteoblastic activity.

In vivo *biocompatibility*

Macroscopic observation. Animals recovered uneventfully postsurgery. Macroscopic infection was not evident at implant sites. No side effects or death were experienced. The soft tissue wounds healed without showing any clinical

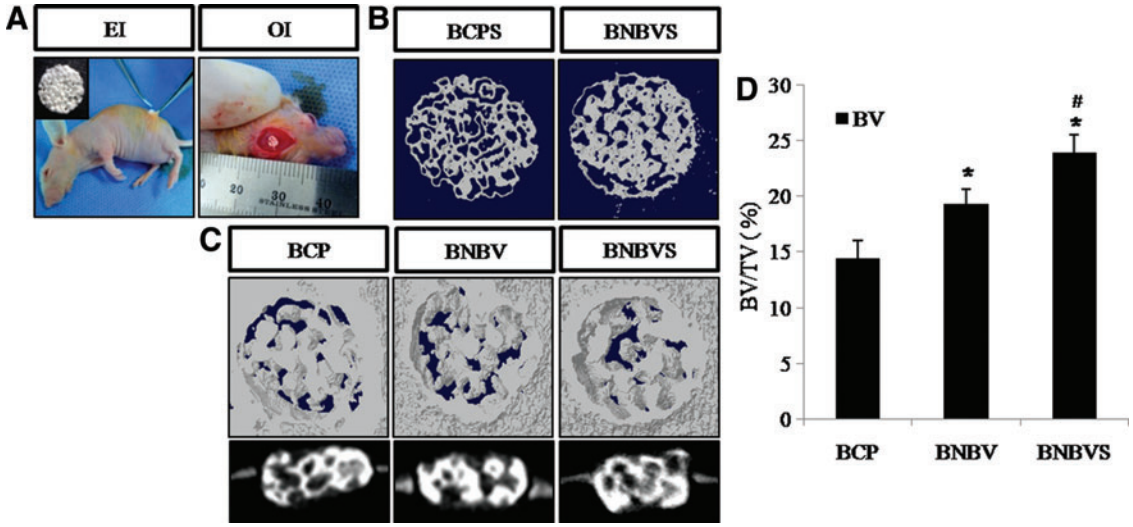

FIG. 6. **(A)** Implant placement at ectopic and orthotopic sites, **(B)** 3D micro-CT images of ectopic implants, **(C)** 3D and 2D cross-sectional micro-CT images of orthotopic implants, **(D)** quantitative analysis of percent bone volume (BV/TV%) at the defect sites at 4 weeks of implantation. BCPS, BCP scaffolds seeded with stem cells; BNBVS, BNBV scaffolds seeded with stem cells; EI, ectopic implantation; OI, orthotopic implantation. $^{*}p<0.05$ versus BCP scaffolds, $^{\#}p<0.05$ versus BNBV scaffolds. BV, bone volume; TV, tissue volume. Color images available online at www.liebertpub.com/tea

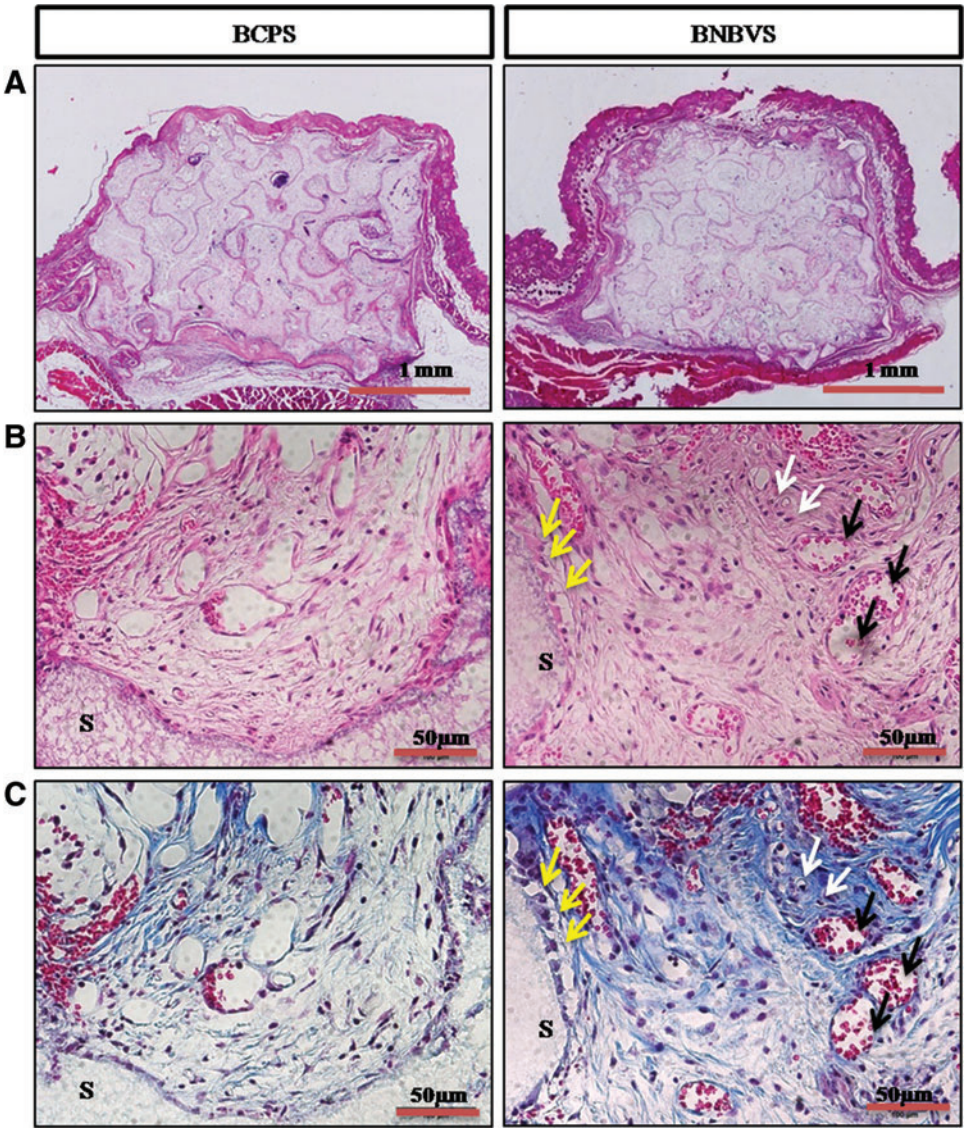

FIG. 7. Histological sections of scaffolds implanted at ectopic sites at 4 weeks stained by hematoxylin and eosin (H&E) method **(A)** whole scaffolds, **(B)** inside the scaffold (enlarged) and Masson's trichrome (M-T) method **(C)** inside the scaffold (enlarged); *white arrows* indicate osteocytes (*black*) inside soft collagen tissue (*blue*), *black arrows* indicate newly formed blood vessels, *yellow arrows* indicate osteoblasts attached to scaffold frame, S indicates scaffold frame. BCPS, BCP scaffolds with differentiated stem cells; BNBVS, BNBV scaffolds with differentiated stem cells. Color images available online at www.liebertpub.com/tea

signs of inflammation in all animals of experimental and control groups.

Micro-CT analysis. Figure 6 showed the micro-CT reconstructions of 4-week-old ectopic implants. The porous morphology of the scaffolds was maintained in all conditions (Fig. 6B, C). 2D cross-sectional and 3D micro-CT images of the orthotopic implants at 4 weeks showed the osteointegration between the implants and the host osseous tissue (Fig. 6C). Quantification of newly formed bone showed that the percent bone volume (BV/TV%) was (14.40 ± 1.62)% in BCP scaffolds, (19.27 ± 1.37)% in BNBV scaffolds, and (24.52 ± 0.71)% in RBMSCs-loaded BNBV scaffolds after 4 weeks (Fig. 6D). This result demonstrated a positive effect of BMP2 and VEGF in improved bone formation within a short period of time and that the presence of stem cells along with growth factors provided the best result.

Histological analysis. Histological examination was performed from ectopic implants extracted from nude mouse back at 4 weeks of implantation. The scaffolds and its porosity were clearly visible with a minimum resorption rate (Fig. 7A). Connective tissue from the thin fibrous capsule grew inside the interconnected pores of the scaffolds (Fig. 7B, C). In some areas of cellular connective tissue, some delicate collagen fibers (blue) with plump osteoblasts were found within the pores of BNBV scaffolds (Fig. 7C, white arrows). A few numbers of osteoblasts were in direct contact with the scaffolds (Fig. 7B, C, yellow arrows). Presence of a higher number of blood vessels inside the pores revealed the effect of VEGF on endothelialization (Fig. 7B, C, black arrows). No typical osteoid depositions or bone formation were seen in BCP scaffolds with or without growth factors. Histological staining confirmed the bone formation observed by micro-CT in the orthotopic sites (nude mouse skull) at 4 weeks. Scaffolds were partially degraded and resorbed (Fig. 8A). Bone formation began at the periphery and progressed to the centers of the BNBV scaffolds (Fig. 8A–C). Stem cell-loaded BNBV implants showed extensive woven and lamellar bone formation at the periphery (Figs. 8B and 9A) and inside the pores of the scaffolds (Figs. 8C and 9B). At the interface region, a

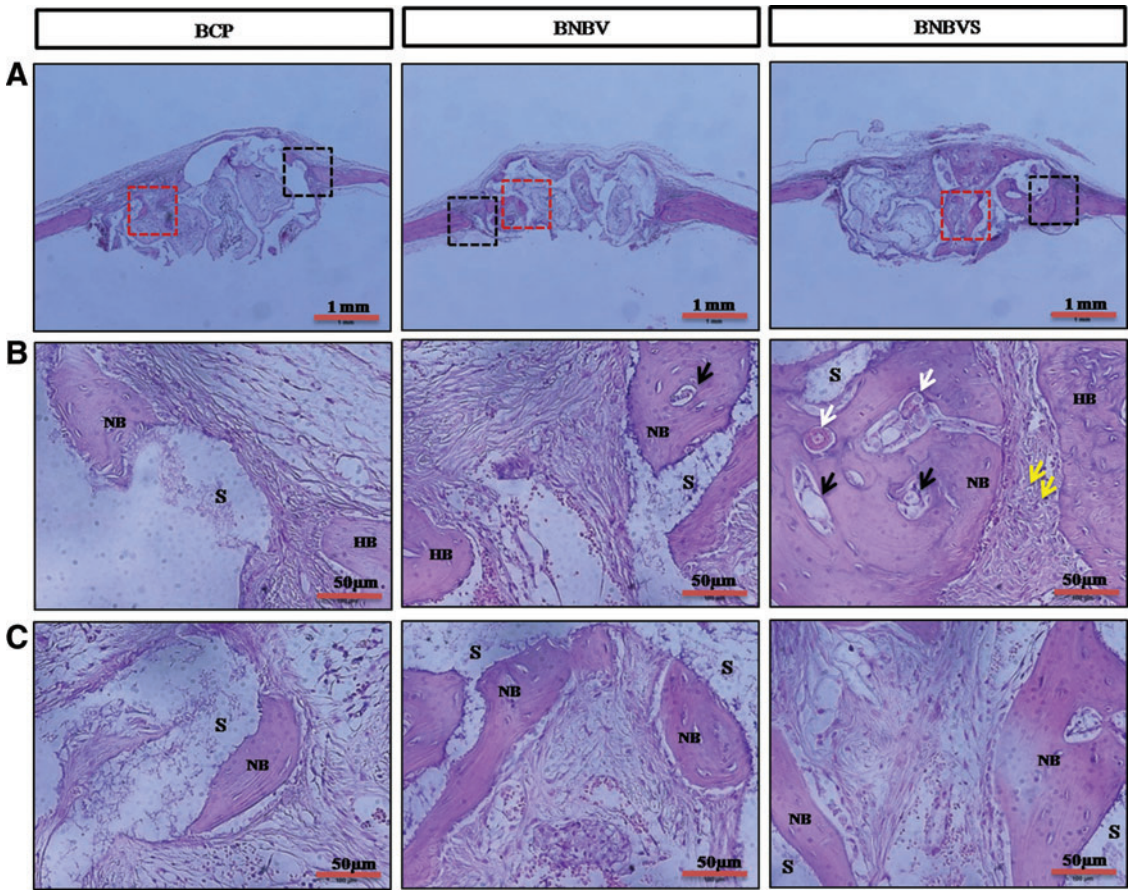

FIG. 8. Histological sections of scaffolds implanted at orthotopic (nude mouse skull) sites at 4 weeks stained by H&E method **(A)** whole scaffolds, *black squares* indicate interface region, *red squares* indicate the inside of the scaffolds; **(B)** interface region (enlarged), **(C)** inside the scaffold (enlarged); NB indicates newly formed bone, HB indicates host bone, *white arrows* indicate newly formed mature blood vessels, *black arrows* indicate newly formed immature blood vessels, *yellow arrows* indicate osteoblasts inside the collagen bundle at interface, S indicates scaffold frame. BNBVS, stem cell-loaded BNBV scaffolds. Color images available online at www.liebertpub.com/tea

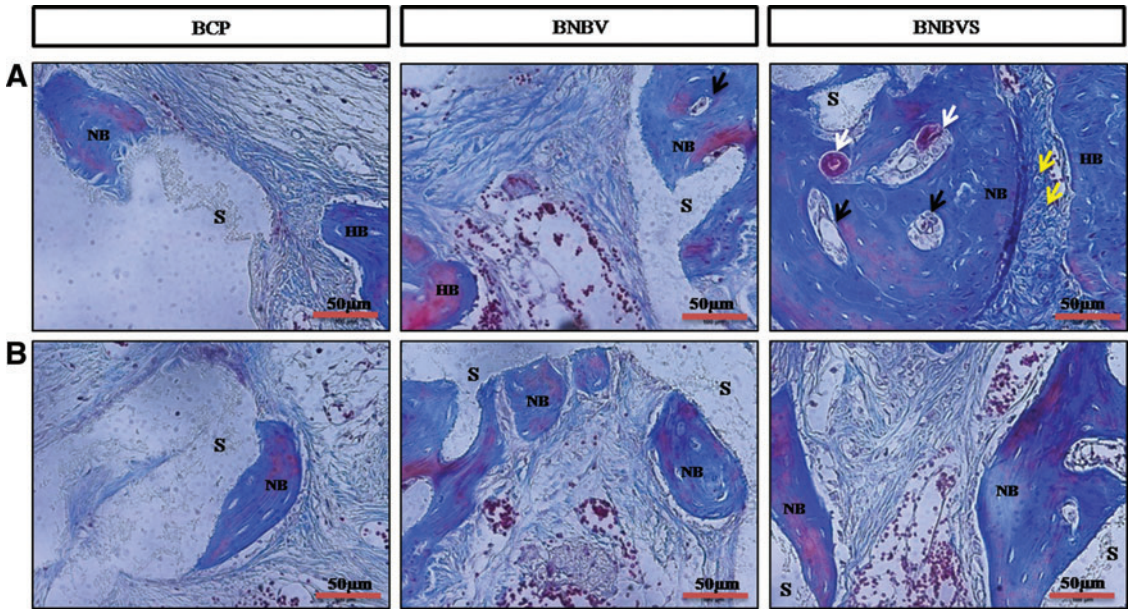

FIG. 9. Histological sections of scaffolds implanted at orthotopic (nude mouse skull) sites at 4 weeks stained by M-T method **(A)** Interface region (enlarged), **(B)** inside the scaffold (enlarged); NB indicates newly formed bone, HB indicates host bone, *white arrows* indicate newly formed mature blood vessels, *black arrows* indicate newly formed immature blood vessels, *yellow arrows* indicate osteoblasts inside the collagen bundle at interface, S indicates scaffold frame. BNBVS, stem cell-loaded BNBV scaffolds. Color images available online at www.liebertpub.com/tea

narrow nonosseous area was observed with dense collagen bundle containing osteoblasts (Figs. 8B and 9A, yellow arrows) within the stem cell-loaded BNBV scaffolds, showing the signs of future ossification (Figs. 8B and 9A). Newly formed bone inside the pore was in direct contact with the scaffolds, indicating higher interaction and osteointegration between new bone and scaffold materials. Blood vessels of different diameter were identified inside the newly formed bone in BNBV and stem cell-loaded BNBV scaffolds. Most of the vessels were consisted of only an endothelial layer (Figs. 8B and 9A, black arrows). Some vessels in stem cell-loaded BNBV scaffolds showed maturation as characterized by the presence of tunica media (Figs. 8B and 9A, white arrows). The remaining parts of these implants were also filled with well-vascularized connective tissue. At the periphery, there was no fibrous tissue barrier between the scaffolds and native bone. No inflammatory response was encountered at the outer surface of the scaffolds and scaffold–host bone interface. Bone formation was lower in the bare BCP scaffolds with decreased number of newly formed blood vessels. This result suggested that BNBV scaffolds had a positive influence on bone formation and addition of stem cells further increased the potentiality of the scaffolds.

Discussion

Multiple signaling molecules, extracellular matrix molecules, and cells interact during the bone healing process.[41,42] Growth factors that stimulate cell growth, differentiation, and vascularization have become a common applicable tool to induce bone formation. Several ceramic, polymer, composite systems have been adapted to maximize their therapeutic potential at the target site. In this study, we designed a new 3D scaffold system provided by sustainable growth factor release properties together with its osteoconductive porous microstructure. NC was considered to be used as a drug carrier in the porous BCP scaffolds for its slow degradation rate with the nano fibrous structure. We evaluated the growth factor-releasing ability of NC and how the released BMP2-VEGF from BNBV scaffolds effected osteogenesis and vasculogenesis and eventually bone formation.

Primarily a highly porous BCP scaffold was fabricated using replica method. The relationship between higher porosity and enhanced bone formation was consistent with previous reports.[43,44] A high degree of porosity allows the delivery of nutrients to the attached cells and provides space for cell proliferation. At the same time a considerable amount of compressive strength is necessary to withhold the pressure inside the body. Although the compressive strength of the porous BCP scaffold was not so good, after loading of NC it was increased considerably with a little decrease in the pore size and porosity. Densely packed glucan chain structure in cellulose fibers lends sufficient mechanical strength to support cell aggregate structures.[45,46] NC-loaded porous scaffold was formed with both macro and micropores (Fig. 1H). The presence of these types of porosity is beneficial for new bone formation where large pores provide space for cell adhesion and proliferation; and small pores help in vascularization.[39,47] Reduction in macropore size and porosity to 150–250 μm and 86.8% did not show any negative effect on cell invasion. Minimum requirement for pore size is considered to be $\sim$100 μm for cell invasion, proliferation, and migration.[43,48] Scaffolds with 150–200 μm pore size and 65% porosity implanted in dog femur defects showed substantial bone ingrowth.[48] Besides, loaded NC provided additional surface area in the scaffolds for initial cell and protein adhesion.[39] Figure 3B showed that a higher number of cells were attached to BN scaffolds than BCP scaffolds at 1 day. Growth factors were mixed with NC before loading onto the BCP scaffolds for physical entrapment. Sustained BMP2 and VEGF release can be established by physical entrapment and absorption.[49–51] BMP-2 and/or VEGF release behavior and entrapment capacity of the scaffolds were analyzed from the release profile. The initial release was 3.67% and 4.68% for BMP2 and VEGF, respectively and the release profile showed a sustainable manner up to 30 days. About 31.90% of BMP2 and 33.38% of VEGF were released up to 30 days. The results seemed to correlate with the degradation rate of the BNBV scaffolds. NC served as the drug carrier in the scaffolds. The drugs slowly defused into the surrounding media since cellulose has a slow degradation rate.[14] According to previous reports, NC microparticle matrix and incorporation of NC into hydrogel scaffolds, nanocomposite films enhanced mechanical strength and facilitated sustained release of drugs.[15,46,52] The release behavior obtained from this study was suitable for large defect bone regeneration process, which needs at least 1 month.

The success of bone substitute materials mostly depends on the formation of a biologically stable and strong interface between the implanted materials and host bone. Upon implantation multiple tissue implant interactions take place from initial cell adhesion to subsequent cellular responses.[53] To study the cellular response on the fabricated scaffolds, RBMSCs were cultured on the scaffolds. Our findings confirmed that fabricated scaffolds favored cell adhesion and proliferation. Cellulose fiber has a high density of reactive hydroxyl groups on its surface, which facilitates the immobilization of cell adhesive proteins such as fibronectin.[54] Addition of BMP2 or VEGF enhanced the proliferation, which was highest with the combination of BMP2 and VEGF. BMP2 affects the interactions between the scaffolds and cell surface receptors and activates cell proliferation *via* the MARK Erk pathway.[55] VEGF promotes the proliferation of bone marrow-derived MSCs through the ERK1/2 and AKT-PKC signal pathway.[56,57]

Apart from cell proliferation, BMP2 and VEGF have distinct roles in the differentiation of MSCs to osteoblasts. BMPs initiate their signaling cascade by binding to special cell receptors, which in turn activate the transcription factors responsible for cell proliferation and differentiation.[58] Two crucial transcription factors namely *Runx2* and *Osx*, regulated by growth factors including BMP2, play different roles at different stages of osteoblastic lineage.[59,60] VEGF controls osteoblast differentiation by regulating the levels of the osteoblast transcription factors *Runx2*.[61] To examine the differentiation activities of released BMP2 and VEGF, we performed immunostaining and RT-PCR on cells on the scaffolds. The expressions of ALP and OPN proteins on the cells were observed by immunostaining. Results showed that the green color indicating the protein localization in the cells was more intense on BNBV scaffolds than on BNB and BNV scaffolds at 7 days and increased over time. The protein expressions on BCP and BN scaffolds were lower

than on any scaffold containing growth factors. These results demonstrated that the dual release of BMP2-VEGF from BNBV scaffolds had a booster effect on cell modulation for ALP and OPN protein expression.

Quantitative data on gene expressions obtained from RT-PCR showed that both early stage markers (*ALP* and *OPN*) and late stage marker (*OCN*) were expressed in higher amounts in cells on BNBV scaffolds than on BNB and BNV scaffolds. Gene expressions were upregulated at 14 days on BNBV scaffolds with an increased fold difference. ALP is the most recognized marker of bone neogenesis. This membrane-bound protein is expressed at the early stage of mineralization, generally, within 14 days of wounding.[62,63] OPN is a noncollagenous protein that contributes to improved bone matrix quality. It promotes the binding between collagen and hydroxyapatite.[64,65] *OCN* expression was lower than *ALP* and *OPN* expressions on the scaffolds at 7 days but it was increased at 14 days. OCN is another calcium-binding protein expressed at the terminal stage of mineralization from mature osteoblasts.[66] Gene expressions were lower on BCP and BN scaffolds than growth factor containing groups. Our finding confirmed that the dual delivery of BMP2-VEGF from BNBV scaffolds accelerated both early and late stage osteoblast differentiation.

In vitro data revealed that growth factors released from NC were able to enhance cell proliferation and differentiation, and BNBV scaffolds had improved biocompatibility than BNB and BNV scaffolds. Therefore, to test the *in vivo* efficiency of BNBV scaffolds, we implanted it ectopically and orthotopically in an animal model for 4 weeks. Previous studies demonstrated that the application of dual growth factor in ectopic and orthopic site increased the bone formation significantly.[28,29] In the ectopic implantation site although increased number of blood vessels proved the effect of VEGF on endothelialization, no typical osteoid formation was evident in BNBV scaffolds. Presence of a few number of osteoblasts adjacent to the scaffolds and inside some soft collagen tissue areas indicated future ossification. It appeared from the findings that enhanced effect of BMP2-VEGF combination was time dependent. These findings may also have resulted from insufficient drug release. Previous study reported that release profiles of BMP2-VEGF significantly changed upon implantation.[29]

In the orthotopic sites, scaffolds showed partial degradation. Osteoblasts migrated to the scaffolds from native bone via scaffold–host bone interface. Bone formation started at the outer surface of the scaffolds and proceeded to the inner pores. Newly formed bone inside the porous structure was in direct contact with the scaffold materials, indicating a high interaction and osteintegration between the scaffolds and the host bone. In some parts, scaffolds were resorbed by the newly deposited bone. BCP scaffolds offered an osteomimetic surface onto which bone matrix deposition occurred layer over layer.[67] The process of osteointegration, together with resorption of scaffold materials, showed the potentiality of the scaffolds to be completely replaced by natural bone over time. At 4 weeks, a higher amount of bone formation was observed in BNBV scaffolds than in BCP scaffolds. This result suggested that amount of released drug from NC was able to accelerate the bone healing mechanism. An increase in vasculature formation in newly deposited bone matrix and connective tissue inside the pores visualized the angiogenic effect of released VEGF. VEGF also served as a chemoattractant [68] and promoted differentiation of osteoblasts.[69,70] These properties of VEGF helped to promote BMP2 induced bone formation. In stem cell-loaded BNBV scaffolds, the extent of bone and vessel formation increased even more at 4 weeks. Kanczler *et al.*[34] reported similar finding when stem cell-loaded scaffolds were implanted into a critical sized femur defect. One previous study showed that BMSCs differentiated to osteogenic lineage in osteogenic medium and thereby accelerated bone formation.[71] Local bone defects were repaired through site-specific delivery of MSCs in an appropriate carrier.[72] Dual delivery of BMP2-transfected BMSCs and platelet-derived growth factor induced excellent new bone formation in rat calvarial defects.[73] Newly deposited bone was integrated with the scaffold frame inside the porous microstructure. Furthermore, a collagen-rich nonosseous area containing osteoblasts were observed between the newly formed bone in the scaffold pores and the extended part of native bone. This finding indicated the preliminary stage of osteointegration between the scaffold bone and host bone. Majority of blood vessels generated in stem cell-loaded BNBV scaffolds were immature with the presence of only an endothelial layer. Some vessels reached maturation as characterized by the presence of tunica media. Induction of blood supply in defect site provided food and nutrients to the cells. Besides, endothelial cells in close contact with stem cells modulated their proliferation and differentiation by signaling interactions.[25] Our results indicated that differentiation of loaded stem cells to osteoblasts by BMP2 and angiogenesis facilitated by VEGF resulted in increased bone formation in stem cell-loaded BNBV scaffolds. The absence of an intermediate fibrous layer barrier and inflammatory reaction at the scaffold–host bone interface provided further proof of better connectivity between the implanted scaffolds and host bone.

Conclusions

In summary, this study evaluated the effects of dual release of BMP2 and VEGF from a new 3D scaffold system (BNBV scaffolds). The sustained release of growth factors positively influenced the proliferation and differentiation of RBMSCs. Although the dual release did not show satisfactory effect on ectopic bone formation at 4 weeks, bone formation was considerably higher in the orthotopic site at the same period of time. RBMSCs seeded on scaffolds further enhanced the bone healing process. These results suggest that NC is a potential carrier for growth factors and BNBV scaffolds seeded with stem cells can be potentially considered for bone tissue engineering.

Acknowledgments

This study was supported by the grants of the Korean Forest Research Institute (FP0400-2013-03), Korea Health Technology R&D project, Ministry of Health and Welfare, Republic of Korea (A111084), and was partially supported by Soonchunhyang University research fund. The authors would also like to thank Mr. Shin-Woo Kim for his contributions to the *in vivo* study.

Disclosure Statement

No competing financial interests exist.

References

1. Sommerfeldt, D., and Rubin, C. Biology of bone and how it orchestrates the form and function of the skeleton. Eur Spine J **10,** S86, 2001.
2. Doblaré, M., Garcıa, J., and Gómez, M. Modelling bone tissue fracture and healing: a review. Eng Fract Mech **71,** 1809, 2004.
3. Ramay, H.R., and Zhang, M. Biphasic calcium phosphate nanocomposite porous scaffolds for load-bearing bone tissue engineering. Biomaterials **25,** 5171, 2004.
4. Bose, S., and Tarafder, S. Calcium phosphate ceramic systems in growth factor and drug delivery for bone tissue engineering: a review. Acta Biomater **8,** 1401, 2012.
5. Wang, C., Varshney, R.R., and Wang, D.-A. Therapeutic cell delivery and fate control in hydrogels and hydrogel hybrids. Adv Drug Deliv Rev **62,** 699, 2010.
6. Drury, J.L., and Mooney, D.J. Hydrogels for tissue engineering: scaffold design variables and applications. Biomaterials **24,** 4337, 2003.
7. Klemm, D., Kramer, F., Moritz, S., Lindström, T., Ankerfors, M., Gray, D., and Dorris, A. Nanocelluloses: a new family of nature-based materials. Angew Chem Int Ed Engl **50,** 5438, 2011.
8. Ben-David, D., Kizhner, T.A., Kohler, T., Müller, R., Livne, E., and Srouji, S. Cell-scaffold transplant of hydrogel seeded with rat bone marrow progenitors for bone regeneration. J Craniomaxillofac Surg **39,** 364, 2011.
9. Weinand, C., Pomerantseva, I., Neville, C.M., Gupta, R., Weinberg, E., Madisch, I., Shapiro, F., Abukawa, H., Troulis, M.J., and Vacanti, J.P. Hydrogel-β-TCP scaffolds and stem cells for tissue engineering bone. Bone **38,** 555, 2006.
10. Bhattacharya, M., Malinen, M.M., Lauren, P., Lou, Y.-R., Kuisma, S.W., Kanninen, L., Lille, M., Corlu, A., GuGuen-Guillouzo, C., and Ikkala, O. Nanofibrillar cellulose hydrogel promotes three-dimensional liver cell culture. J Control Release **164,** 291, 2012.
11. Linh, N.T.B., Min, Y.K., and Lee, B.-T. Fabrication and *in vitro* evaluations with osteoblast-like MG-63 cells of porous hyaluronic acid-gelatin blend scaffold for bone tissue engineering applications. J Mater Sci **48,** 4233, 2013.
12. Cheng, Y., Luo, X., Payne, G.F., and Rubloff, G.W. Biofabrication: programmable assembly of polysaccharide hydrogels in microfluidics as biocompatible scaffolds. J Mater Chem **22,** 7659, 2012.
13. Pääkkö, M., Ankerfors, M., Kosonen, H., Nykänen, A., Ahola, S., Österberg, M., Ruokolainen, J., Laine, J., Larsson, P., and Ikkala, O. Enzymatic hydrolysis combined with mechanical shearing and high-pressure homogenization for nanoscale cellulose fibrils and strong gels. Biomacromolecules **8,** 1934, 2007.
14. Entcheva, E., Bien, H., Yin, L., Chung, C.-Y., Farrell, M., and Kostov, Y. Functional cardiac cell constructs on cellulose-based scaffolding. Biomaterials **25,** 5753, 2004.
15. Kolakovic, R., Laaksonen, T., Peltonen, L., Laukkanen, A., and Hirvonen, J. Spray-dried nanofibrillar cellulose microparticles for sustained drug release. Int J Pharm **430,** 47, 2012.
16. Andersson, J., Stenhamre, H., Bäckdahl, H., and Gatenholm, P. Behavior of human chondrocytes in engineered porous bacterial cellulose scaffolds. J Biomed Mater Res Part A **94,** 1124, 2010.
17. Heckman, J.D., Ehler, W., Brooks, B.P., Aufdemorte, T.B., Lohmann, C.H., Morgan, T., and Boyan, B.D. Bone morphogenetic protein but not transforming growth factor-β enchances bone formation in canine diaphyseal nonunions implanted with a biodegradable composite polymer. J Bone Joint Surg **81,** 1717, 1999.
18. Street, J., Bao, M., Bunting, S., Peale, F.V., Ferrara, N., Steinmetz, H., Hoeffel, J., Cleland, J.L., Daugherty, A., and van Bruggen, N. Vascular endothelial growth factor stimulates bone repair by promoting angiogenesis and bone turnover. Proc Natl Acad Sci U S A **99,** 9656, 2002.
19. Eckardt, H., Ding, M., Lind, M., Hansen, E.S., Christensen, K., and Hvid, I. Recombinant human vascular endothelial growth factor enhances bone healing in an experimental nonunion model. J Bone Joint Surg Br **87,** 1434, 2005.
20. Kent Leach, J., Kaigler, D., Wang, Z., Krebsbach, P.H., and Mooney, D.J. Coating of VEGF-releasing scaffolds with bioactive glass for angiogenesis and bone regeneration. Biomaterials **27,** 3249, 2006.
21. Simón-Yarza, T., Tamayo, E., Benavides, C., Lana, H., Formiga, F.R., Grama, C.N., Ortiz-de-Solorzano, C., Kumar, M.N.V.R., Prosper, F., and Blanco-Prieto, M.J. Functional benefits of PLGA particulates carrying VEGF and CoQ10 in an animal of myocardial ischemia. Int J Pharm **454,** 784, 2013.
22. Kim, B.R., Nguyen, L.T., Min, Y.K., and Lee, B.T. *In vitro* and *in vivo* studies of BMP-2 loaded PCL-Gelatin-BCP electrospun scaffolds. Tissue Eng Part A **20,** 3279, 2014.
23. Wozney, J.M. Overview of bone morphogenetic proteins. Spine **27,** S2, 2002.
24. Kaigler, D., Krebsbach, P.H., Polverini, P.J., and Mooney, D.J. Role of vascular endothelial growth factor in bone marrow stromal cell modulation of endothelial cells. Tissue Eng **9,** 95, 2003.
25. Guillotin, B., Bareille, R., Bourget, C., Bordenave, L., and Amedee, J. Interaction between human umbilical vein endothelial cells and human osteoprogenitors triggers pleiotropic effect that may support osteoblastic function. Bone **42,** 1080, 2008.
26. Carano, R.A.D., and Filvaroff, E.H. Angiogenesis and bone repair. Drug Discov Today **8,** 980, 2003.
27. Peng, H., Usas, A., Olshanski, A., Ho, A.M., Gearhart, B., Cooper, G.M., and Huard, J. VEGF improves, whereas sFlt1 inhibits, BMP2-induced bone formation and bone healing through modulation of angiogenesis. J Bone Miner Res **20,** 2017, 2005.
28. Patel, Z.S., Young, S., Tabata, Y., Jansen, J.A., Wong, M.E., and Mikos, A.G. Dual delivery of an angiogenic and an osteogenic growth factor for bone regeneration in a critical size defect model. Bone **43,** 931, 2008.
29. Kempen, D.H., Lu, L., Heijink, A., Hefferan, T.E., Creemers, L.B., Maran, A., Yaszemski, M.J., and Dhert, W.J. Effect of local sequential VEGF and BMP-2 delivery on ectopic and orthotopic bone regeneration. Biomaterials **30,** 2816, 2009.
30. Yun, Y.-R., Jang, J.H., Jeon, E., Kang, W., Lee, S., Won, J.-E., Kim, H.W., and Wall, I. Administration of growth factors for bone regeneration. Regen Med **7,** 369, 2012.
31. Kon, E., Muraglia, A., Corsi, A., Bianco, P., Marcacci, M., Martin, I., Boyde, A., Ruspantini, I., Chistolini, P., and Rocca, M. Autologous bone marrow stromal cells loaded onto porous hydroxyapatite ceramic accelerate bone repair

in critical-size defects of sheep long bones. J Biomed Mater Res **49,** 328, 2000.
32. Yamada, Y., Seong Boo, J., Ozawa, R., Nagasaka, T., Okazaki, Y., Hata, K.-i., and Ueda, M. Bone regeneration following injection of mesenchymal stem cells and fibrin glue with a biodegradable scaffold. J Craniomaxillofac Surg **31,** 27, 2003.
33. Roldán, J., Detsch, R., Schaefer, S., Chang, E., Kelantan, M., Waiss, W., Reichert, T., Gurtner, G., and Deisinger, U. Bone formation and degradation of a highly porous biphasic calcium phosphate ceramic in presence of BMP-7, VEGF and mesenchymal stem cells in an ectopic mouse model. J Craniomaxillofac Surg **38,** 423, 2010.
34. Kanczler, J.M., Ginty, P.J., White, L., Clarke, N.M., Howdle, S.M., Shakesheff, K.M., and Oreffo, R.O. The effect of the delivery of vascular endothelial growth factor and bone morphogenic protein-2 to osteoprogenitor cell populations on bone formation. Biomaterials **31,** 1242, 2010.
35. Lee, S.-Y., Chun, S.-J., Kang, I.-A., and Park, J.-Y. Preparation of cellulose nanofibrils by high-pressure homogenizer and cellulose-based composite films. J Ind Eng Chem **15,** 50, 2009.
36. Kim, M., Franco, R.A., and Lee, B.-T. Synthesis of functional gradient BCP/ZrO2 bone substitutes using ZrO2 and BCP nanopowders. J Eur Ceram Soc **31,** 1541, 2011.
37. Lee, B.-T., Youn, M.-H., Paul, R.K., Lee, K.-H., and Song, H.-Y. *In situ* synthesis of spherical BCP nanopowders by microwave assisted process. Mater Chem Phys **104,** 249, 2007.
38. Alhadlaq, A., and Mao, J.J. Mesenchymal stem cells: isolation and therapeutics. Stem Cells Dev **13,** 436, 2004.
39. Nguyen, T.B.L., and Lee, B.-T. A combination of biphasic calcium phosphate scaffold with hyaluronic acid-gelatin hydrogel as a new tool for bone regeneration. Tissue Eng Part A **20,** 1993, 2014.
40. Nath, S.D., Abueva, C., Kim, B., and Lee, B.T. Chitosan–hyaluronic acid polyelectrolyte complex scaffold crosslinked with genipin for immobilization and controlled release of BMP-2. Carbohydr Polym **115,** 160, 2015.
41. Urist, M.R. Bone: formation by autoinduction. Science **150,** 893, 1965.
42. Deschaseaux, F., Sensébé, L., and Heymann, D. Mechanisms of bone repair and regeneration. Trends Mol Med **15,** 417, 2009.
43. Karageorgiou, V., and Kaplan, D. Porosity of 3D biomaterial scaffolds and osteogenesis. Biomaterials **26,** 5474, 2005.
44. Sun, X., Kang, Y., Bao, J., Zhang, Y., Yang, Y., and Zhou, X. Modeling vascularized bone regeneration within a porous biodegradable CaP scaffold loaded with growth factors. Biomaterials **34,** 4971, 2013.
45. Ko, I.K., and Iwata, H. An approach to constructing three-dimensional tissue. Ann N Y Acad Sci **944,** 443, 2001.
46. Dash, R., Foston, M., and Ragauskas, A.J. Improving the mechanical and thermal properties of gelatin hydrogels cross-linked by cellulose nanowhiskers. Carbohydr Polym **91,** 638, 2013.
47. Bignon, A., Chouteau, J., Chevalier, J., Fantozzi, G., Carret, J.-P., Chavassieux, P., Boivin, G., Melin, M., and Hartmann, D. Effect of micro-and macroporosity of bone substitutes on their mechanical properties and cellular response. J Mater Sci Mater Med **14,** 1089, 2003.
48. Hulbert, S.F., Young, F.A., Mathews, R.S., Klawitter, J.J., Talbert, C.D., and Stelling, F.H. Potential of ceramic materials as permanently implantable skeletal prostheses. J Biomed Mater Res **4,** 433, 1970.
49. Duan, B., and Wang, M. Customized Ca–P/PHBV nanocomposite scaffolds for bone tissue engineering: design, fabrication, surface modification and sustained release of growth factor. J R Soc Interface **7,** S615, 2010.
50. Ma, X., Wu, X., Hu, Y., Xiong, Z., Lv, R., Wang, J., Li, D., and Yan, Y. Intervertebral spinal fusion using a RP-based PLGA/TCP/bBMP biomimetic grafting material. J Bioact Compat Polym **24,** 146, 2009.
51. Yang, P., Wang, C., Shi, Z., Huang, X., Dang, X., Xu, S., and Wang, K. Prefabrication of vascularized porous three-dimensional scaffold induced from rhVEGF165: a preliminary study in rats. Cells Tissues Organs **189,** 327, 2008.
52. Goetz, L., Mathew, A., Oksman, K., Gatenholm, P., and Ragauskas, A.J. A novel nanocomposite film prepared from crosslinked cellulosic whiskers. Carbohydr Polym **75,** 85, 2009.
53. Puleo, D.A., and Nanci, A. Understanding and controlling the bone–implant interface. Biomaterials **20,** 2311, 1999.
54. Noiset, O., Schneider, Y.-J., and Marchand-Brynaert, J. Fibronectin adsorption or/and covalent grafting on chemically modified PEEK film surfaces. J Biomater Sci Polym Ed **10,** 657, 1999.
55. Rodrigues, M., Griffith, L.G., and Wells, A. Growth factor regulation of proliferation and survival of multipotential stromal cells. Stem Cell Res Ther **1,** 32, 2010.
56. Kong, X., Zheng, F., Guo, L., Yang, J., Zhang, L., Tang, J., Huang, Y., and Wang, J. [VEGF promotes the proliferation of bone marrow derived mesenchymal stem cells through ERK1/2 signal pathway]. Zhongguo Shi Yan Xue Ye Xue Za Zhi = J Exp Hematol **18,** 1292, 2010 [Article in Chinese].
57. Zhang, J., Xie, S., Han, X., Ren, J., Lv, F., Tang, J., Zheng, F., Guo, L., Yang, J., and Kong, X. [Effect of vascular endothelial growth factor on bone marrow-derived mesenchymal stem cell proliferation and the signaling mechanism]. Nan Fang Yi Ke Da Xue Xue Bao = J South Med Univ **31,** 1697, 2011 [Article in Chinese].
58. Luu, H.H., Song, W.X., Luo, X., Manning, D., Luo, J., Deng, Z.L., Sharff, K.A., Montag, A.G., Haydon, R.C., and He, T.C. Distinct roles of bone morphogenetic proteins in osteogenic differentiation of mesenchymal stem cells. J Orthop Res **25,** 665, 2007.
59. Gordeladze, J.O., Reseland, J.E., Duroux-Richard, I., Apparailly, F., and Jorgensen, C. From stem cells to bone: phenotype acquisition, stabilization, and tissue engineering in animal models. ILAR J **51,** 42, 2010.
60. Komori, T. Regulation of bone development and maintenance by Runx2. Front Biosci **13,** 898, 2007.
61. Berendsen, A.D., and Olsen, B.R. How vascular endothelial growth factor-a (VEGF) regulates differentiation of mesenchymal stem cells. J Histochem Cytochem **62,** 103, 2014.
62. Allen, M.J. Biochemical markers of bone metabolism in animals: uses and limitations. Vet Clin Pathol **32,** 101, 2003.
63. Stucki, U., Schmid, J., Hammerle, C.F., and Lang, N.P. Temporal and local appearance of alkaline phosphatase activity in early stages of guided bone regeneration. A descriptive histochemical study in humans. Clin Oral Implants Res **12,** 121, 2001.
64. Chen, Y., Bal, B.S., and Gorski, J.P. Calcium and collagen binding properties of osteopontin, bone sialoprotein, and bone acidic glycoprotein-75 from bone. J Biol Chem **267,** 24871, 1992.

65. Stayton, P.S., Drobny, G.P., Shaw, W.J., Long, J.R., and Gilbert, M. Molecular recognition at the protein-hydroxyapatite interface. Crit Rev Oral Biol Med **14,** 370, 2003.
66. Malaval, L., Liu, F., Roche, P., and Aubin, J.E. Kinetics of osteoprogenitor proliferation and osteoblast differentiation *in vitro*. J Cell Biochem **74,** 616, 1999.
67. Boyde, A., Corsi, A., Quarto, R., Cancedda, R., and Bianco, P. Osteoconduction in large macroporous hydroxyapatite ceramic implants: evidence for a complementary integration and disintegration mechanism. Bone **24,** 579, 1999.
68. Mayr-Wohlfart, U., Waltenberger, J., Hausser, H., Kessler, S., Günther, K.-P., Dehio, C., Puhl, W., and Brenner, R. Vascular endothelial growth factor stimulates chemotactic migration of primary human osteoblasts. Bone **30,** 472, 2002.
69. Deckers, M.M., Karperien, M., van der Bent, C., Yamashita, T., Papapoulos, S.E., and Löwik, C.W. Expression of vascular endothelial growth factors and their receptors during osteoblast differentiation. Endocrinology **141,** 1667, 2000.
70. Midy, V., and Plouét, J. Vasculotropin/vascular endothelial growth factor induces differentiation in cultured osteoblasts. Biochem Biophys Res Commun **199,** 380, 1994.
71. Krebsbach, P., Kuznetsov, S.A., Bianco, P., and Robey, P.G. Bone marrow stromal cells: characterization and clinical application. Crit Rev Oral Biol Med **10,** 165, 1999.
72. Bruder, S.P., Fink, D.J., and Caplan, A.I. Mesenchymal stem cells in bone development, bone repair, and skeletal regenaration therapy. J Cell Biochem **56,** 283, 1994.
73. Park, S.-Y., Kim, K.-H., Shin, S.-Y., Koo, K.-T., Lee, Y.-M., and Seol, Y.-J. Dual delivery of rhPDGF-BB and bone marrow mesenchymal stromal cells expressing the BMP2 gene enhance bone formation in a critical-sized defect model. Tissue Eng Part A **19,** 2495, 2013.

Address correspondence to:
Byong-Taek Lee, PhD
Department of Regenerative Medicine
College of Medicine
Soonchunhyang University
366-1 Ssangyong dong
Cheonan 330-090
Chungnam
Republic of Korea

E-mail: lbt@sch.ac.kr

Received: August 19, 2014
Accepted: February 23, 2015
Online Publication Date: April 29, 2015